Renewable and Sustainable Energy Reviews 16 (2012) 29–36

Contents lists available at SciVerse ScienceDirect

Renewable and Sustainable Energy Reviews

journal homepage: www.elsevier.com/locate/rser

Development of a simulation model for a three-dimensional wind velocity field using Ténès Algeria as a case study

Fouad Boukli Hacène[a], Miloud Tahar Abbés[b], Nachida Kasbadji Merzouk[c], Larbi Loukarfi[b], Hacene Mahmoudi[a,c,*], Matheus F.A. Goosen[d]

[a] Faculty of Sciences, University Hassiba Benbouli, Bp 151, Chlef, Algeria
[b] Faculty of Technology, University Hassiba Benbouli, Bp 151, Chlef, Algeria
[c] Solar Equipments Development Unit (UDES), Center for Renewable Energies Development (CDER), BP. 386, Bou-Ismail, 42415, Tipaza, Algeria
[d] Alfaisal University, Riyadh, Saudi Arabia

ARTICLE INFO

Article history:
Received 12 April 2011
Accepted 5 July 2011
Available online 15 September 2011

Keywords:
Constraint method
Mass-consistent method
Adjusted velocities
Wind fields simulation
Finite difference method
Complex terrain

ABSTRACT

A mathematical simulation model was developed that can determine the three-dimensional wind velocity field over a complex terrain. The Ténès area in the Valley of Cheliff in Algeria was used as a case study. This region is exposed to south-west circulation that makes it favorable to the use of wind energy. Knowledge of wind fields is crucial for predicting the dispersion of pollutants, for forecasting meteorological weather, for fire spread prediction and in the design and implementation of wind turbines. By means of a mass consistent model, an in-house program was developed to calculate the three-dimensional wind velocity field in the study region. The model was supported by a numerical box in which flow through is allowed for in the upper and lateral boundaries. The bottom boundary through which no flow through occurs was determined by the topographic relief at the surface. From measured wind velocities, observed values were calculated by interpolation–extrapolation. Using an optimization method, the adjusted velocities were obtained from constraints, observed velocities and the continuity equation. The model was verified with wind point data, the relative error did not exceed 6%.

Contents

1. Introduction

The interest in wind energy production has increased considerably due to improvements in turbine technology and the growing need for power production from renewable sources [1–3]. One of the most important issues to deal with is the choice of an adequate site for a wind farm [4]. Different methodologies have been developed to investigate and define the wind climate of regions using

* Corresponding author at: Faculty of Sciences, University Hassiba Benbouli, Bp 151, Chlef, Algeria.
E-mail address: usto98@yahoo.fr (H. Mahmoudi).

1364-0321/$ – see front matter © 2011 Elsevier Ltd. All rights reserved.
doi:10.1016/j.rser.2011.07.133

Nomenclature

λ	Lagrange multiplier
σ_i	variances of the observed field
α_i	Gauss precision module
F	objective function
V	Computational domain
u^0, v^0 and w^0	fixed observed velocity value in x, y and z direction
u, v and w	velocity adjusted value in x, y and z direction
Δx, Δy, Δz	step in x, y and z direction

actual measured data [5]. Mortensen and Petersen [6] for example have shown that numerical models are suitable for simulating wind fields. Such models can indicate the best sites for installation of wind turbines.

Due to a boost in the world's energy consumption as a result of population growth and industrialization, renewable energy (i.e. solar, wind, geothermal and wave) has increased in importance [7]. A study by Ludwig and Byrd [8] has shown that meteorological and air pollution problems frequently require the interpolation of complete, three-dimensional wind field flows from a limited number of observations at specific location. Modeling atmospheric flow is difficult, especially when simulating wind fields over irregular terrain [9].

Different types of wind field models have been developed in the last few years [10]. They can be classified into two main models: diagnostic (kinetic) and prognostic (dynamic). Kinetic models are those capable of reconstructing a steady-state wind field starting from a set of initial experimental data. Their equations contain no time dependent terms. On the other hand, dynamic models describe the time evolution of meteorologically variable fields starting from an initial state and merging the effects of possible time variations of boundary conditions.

Diagnostic (i.e. kinetic) models follow two main approaches [11]: a linearized model which is a simplified steady-state solution of the Navier–Stokes equation, and the mass-consistent model which analyses available meteorological data, with physical constraints like mass-conservation. It is a general practice to use mass consistent models for simulation of stationary three-dimensional wind fields in complex terrain. The advantage of a mass consistent model compared with primitive equation models is the relatively short computing time. However, as a result it is not possible to look at complex phenomenon such as turbulence [12].

The implementation of a mass consistent wind field is typically undertaken using available meteorological data. The procedure has been effective for predicting winds for emergency response contaminant dispersion, for weather forecasts, in wind energy studies and for storm flooding prediction [13]. Furthermore, some applications require that the derived wind field be non divergent.

The mass-consistent models reconstruct 3-D wind fields starting from vertical profiles and near-ground wind measurements through a two-step procedure [14]. The observed data needed for the mass consistent model are provided by an interpolation–extrapolation scheme using information available at a given site to determine velocity components at each grid point above the topography. Typically the available simultaneous data consists of several horizontal wind speed and direction measurements near the earth's surface, a vertical profile of horizontal wind speed and direction and synoptic analysis.

The wind data interpolation method plays a crucial role in determining the final wind field features. Different wind fields can be generated starting from the same data and changing only the interpolation method. The adjustment procedure is generally obtained by employing the variational analysis technique [15]. Early research was conducted by Sasaki [16–18] who developed the first theoretical model for the calculation of wind speed. Many different mass-consistent models have been developed starting from the late seventies [19–29]. Various other works relating the results of air pollution dispersion modeling in complex terrain are entirely dependent on adequate descriptions of the three-dimensional wind field [30]. Furthermore, as part of modernization efforts of the Atmospheric Release Advisory Capability (ARAC) project, Chan and Sugiyama [31] developed a new diagnostic model for generating mass consistent wind fields over a continuous terrain. In addition, Leone et al. [32] have used wind fields to drive ARAC's new dispersion model. This model is going to replace the current operational code described by Sherman [19] which employs stair-step topography and constant grid spacing. The topography strongly influences the boundary layer flow in such a manner that the geographic variations either can modify on in some cases generate circulations in conjunction with diurnal heating cycles [33,34].

The theoretical basis for the mass consistent model was developed by Sasaki [16–18]. The general variational analysis formalism defines an integral function whose external solution minimizes the variance of the difference between the observed and analyzed variable values subject to physical constraints which are the continuity equation and the measured velocities.

The aim of this paper is to develop a mathematical simulation model that can determine the three-dimensional wind velocity field over a complex terrain using the Valley of Cheliff in the Tenes area in Algeria as a case study. This region has a complex relief with a set of mountains and valleys with strong slopes. In the adjustment model for wind flow, the relief is analyzed explicitly with the use of velocity measurements in the field using a large number of points in a three-dimensional grid. The data are interpolated and extrapolated by a least squares method on the grid of an Euler model. The numerical results are compared with the measurement values at selected points on the real terrain.

Table 1
Characteristics of the measuring station [19].

Site	Longitude (°)	Latitude (°)	Altitude (M)	Period of measure (year)	Height of mast (m)
Ténès	1.33	36.5	17	5	10

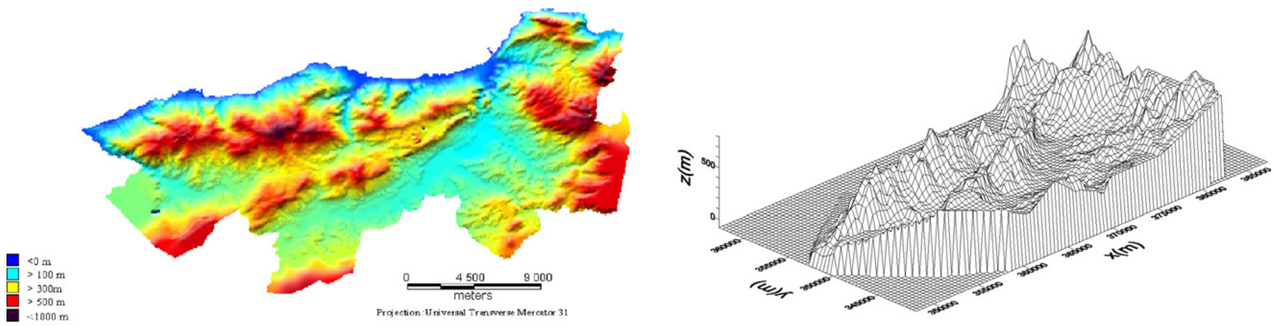
2. Methodology

2.1. Case study area

The study area is located in the town of Tenes in Algeria. It is a coastal city which is partially surrounded by the Dahra mountain range. The topography of this region is complex with a variation in altitude between 0 and 700 m (Fig. 1a). The correspondent mathematical topographic model is given in Fig. 1b. The data file that defines the terrain relief by the three coordinates contains 374,037 points. Digital processing was used to order the relief structure. The site is characterized by an important wind potential area [35]. The weather station at this location has 5 years of continuous measurements of three-hourly speed and wind direction [36]. Characteristics of the measuring station are given in Table 1.

2.2. Mathematical model formulation

The study is presented as an optimization problem with constraint conditions. The objective function is given by an integral



(a) Digital terrain model in the region of Tenes

(b) Relief given by 374037 points

Fig. 1. Digital and mathematical relief of Tenes.

functional [16–18]:

$$E = \int_v (F(u, v, w, \lambda)\, dx\, dy\, dz \tag{1}$$

where F is a function expressed by

$$F(u, v, w, \lambda) = \alpha_1^2(u-u^0)^2 + \alpha_1^2(v-v^0)^2 + \alpha_2^2(w-w^0)^2 + \lambda\left(\frac{\partial u}{\partial x} + \frac{\partial v}{\partial y} + \frac{\partial w}{\partial z}\right) \tag{2}$$

where u, v, and w are the argument functions which represent respectively the components wind velocity in x, y, and z direction of the modeling domain V. The mass consistent model constructs an observed initial guess of the wind velocities component u^0, v^0 and w^0 over the entire model. The initial estimates are formed from an interpolation–extrapolation scheme that uses existing surface wind observations contained within the modeled area. The values u, v and w are obtained by adjusted scheme from the observed velocities by minimizing the functional E. The parameter $\lambda(x, y, z)$ is the Lagrange multiplier; and values of α_i are Gauss precision moduli taken to be $\alpha_i^2 \equiv 1/2\sigma_i^2$. σ_i is an observation error and/or variances of the observed field from the desired adjusted field. Identical Gauss precision moduli are assumed for the horizontal directions. The ratio $\alpha = (\alpha_1/\alpha_2)^2 = (\sigma_2/\sigma_1)^2$ is related to stability and turbulence of atmosphere [19].

The variational calculus gives the Euler–Lagrange equation for u, v and w, respectively [37]:

$$\begin{aligned} \frac{\partial F}{\partial u} - \frac{d}{dx}\left(\frac{\partial F}{\partial u_x}\right) &= 0 \\ \frac{\partial F}{\partial v} - \frac{d}{dy}\left(\frac{\partial F}{\partial v_x}\right) &= 0 \\ \frac{\partial F}{\partial w} - \frac{d}{dz}\left(\frac{\partial F}{\partial w_x}\right) &= 0 \end{aligned} \tag{3}$$

where

$$\begin{aligned} u_x &= \frac{\partial u}{\partial x} \\ u_y &= \frac{\partial v}{\partial y} \\ u_x &= \frac{\partial w}{\partial z} \end{aligned} \tag{4}$$

Eq. (3) are subjected to the boundary conditions:

$$\vec{n}\,\lambda\,\vec{\nabla}U = 0 \tag{5}$$

where $\vec{n}$ is the outward positive unit normal to the boundary of volume V. Eq. (5) implies that on the boundary, either of the following is satisfied:

$$\vec{\nabla}\mathrm{U} = 0 \quad \text{or} \quad \lambda = 0 \tag{6}$$

Eq. (5) represents appropriate conditions for "flow-through" lateral and upper boundaries. Either the normal velocity component variation or λ must be zero on a boundary. The appropriate condition for "flow-through" boundary (upper and lateral boundary) is $\lambda = 0$. In this case the derivate of λ in the direction across the boundary is in general not zero. The lower boundary coincides with the ground and represents a "no-flow-through" solid boundary. The observed velocity at that boundary is zero [19,25,42].

Substituting for F by putting Eq. (2) into Eq. (3), we obtain:

$$\begin{aligned} u &= u^0 + \frac{1}{2\alpha_1^2}\frac{\partial \lambda}{\partial x} \\ v &= v^0 + \frac{1}{2\alpha_1^2}\frac{\partial \lambda}{\partial y} \\ w &= w^0 + \frac{1}{2\alpha_2^2}\frac{\partial \lambda}{\partial z} \end{aligned} \tag{7}$$

The continuity equation is given by:

$$\frac{\partial u}{\partial x} + \frac{\partial v}{\partial y} + \frac{\partial w}{\partial z} = 0 \tag{8}$$

The equation for λ is derived by differentiating Eq. (7) and substituting the results into Eq. (8) giving:

$$\frac{\partial^2 \lambda}{\partial x^2} + \frac{\partial^2 \lambda}{\partial y^2} + \left(\frac{\alpha_1^2}{\alpha_2^2}\right)\frac{\partial^2 \lambda}{\partial z^2} = -2\alpha_1^2\left(\frac{\partial u^0}{\partial x} + \frac{\partial v^0}{\partial y} + \frac{\partial w^0}{\partial z}\right) \tag{9}$$

Eq. (9) is an elliptical differential equation (Poisson's equation). It will be solved for λ with the specific boundary conditions of Eq. (5). The adjusted wind velocity components are calculated using Eq. (7).

2.3. Method of resolution

This case study can be described as a constraint optimized problem where Eq. (1) is the objective function and the constraint conditions are the continuity equation and the measured values in the volume V. Mass-consistent optimization is used to solve the problem. The basic procedure to get the wind field velocities by the mass-consistent method is given by the following steps:

The Lagrange parameter $\lambda_{i,j,k}$ is determined by Eq. (9) by the finite difference method in the discretised volume V which is a rectangular box set on the topographic relief. The grid model is built with a choice of Δx and Δy such that the grid takes in account

the more interesting topographic detail features of the site (e.g. mountains, canyons and valley areas). The computational volume is shown in Fig. 1.

By using a central difference scheme for second derivatives for a grid point (i,j,k), Eq. (9) is rewritten as:

$$\frac{\lambda_{i+1,j,k}-2\lambda_{i,j,k}+\lambda_{i-1,j,k}}{\Delta x^2}+\frac{\lambda_{i,j+1,k}-2\lambda_{i,j,k}+\lambda_{i,j-1,k}}{\Delta y^2}+\left(\frac{\alpha_1^2}{\alpha_2^2}\right)\frac{\lambda_{i,j,k+1}-2\lambda_{i,j,k}+\lambda_{i,j,k-1}}{\Delta z^2}=-2\alpha_1^2\varepsilon_0 \quad (10)$$

With the divergence ε_0 of the interpolated wind field is given by:

$$\varepsilon_0=\frac{\partial u^0}{\partial x}+\frac{\partial v^0}{\partial y}+\frac{\partial w^0}{\partial z} \quad (11a)$$

Using central difference for the first derivate ε_0 is written as:

$$\varepsilon_0=\frac{u^0_{i+1,j,k}-u^0_{i-1,j,k}}{2\Delta x}+\frac{v^0_{i,j+1,k}-v^0_{i,j-1,k}}{2\Delta y}+\frac{w^0_{i,j,k+1}-w^0_{i,j,k-1}}{2\Delta z} \quad (11b)$$

where the observed values $u^0_{i,j,k}$, $v^0_{i,j,k}$ and $w^0_{i,j,k}$ were determined by least square weighted method from the measured wind speed. The method uses the three nearest measured points to determine the observed wind speed at each grid point (i,j,k). Once the observed velocities are determined, ε_0 is introduced in Eq. (10). A set of difference equation in $\lambda_{i,j,k}$ is now obtained at each interior grid point. The entire system is solved simultaneously for the value of $\lambda_{i,j,k}$. The equation set is solved iteratively, using a successive over-relaxation method.

In altitude z the observed values (either measured or adjusted values) are extrapolated with the following equation [38]:

$$\vec{U}=\vec{U}_0\left(\frac{z}{z_0}\right)^p \quad (12)$$

where the exponent p is determined by atmospheric stability conditions or from a least squares fit to multiple level tower data.

Once the Lagrange parameters are determined, the adjusted wind field values are calculated using central difference for $\lambda_{i,j,k}$ and mean value for observed wind value of Eq. (7):

$$\begin{aligned}
u_{i,j,k}&=\frac{1}{4}(u^0_{i+1,j,k}+2u^0_{i,j,k}+u^0_{i-1,j,k})+\frac{1}{2\alpha_1^2}\left(\frac{\lambda_{i+1,j,k}-\lambda_{i-1,j,k}}{2\Delta x}\right)\\
v_{i,j,k}&=\frac{1}{4}(v^0_{i,j+1,k}+2v^0_{i,j,k}+v^0_{i,j-1,k})+\frac{1}{2\alpha_1^2}\left(\frac{\lambda_{i,j+1,k}-\lambda_{i,j-1,k}}{2\Delta y}\right)\\
w_{i,j,k}&=\frac{1}{4}(w^0_{i,j,k+1}+2w^0_{i,j,k}+w^0_{i,j,k-1})+\frac{1}{2\alpha_2^2}\left(\frac{\lambda_{i,j,k+1}-\lambda_{i,j,k-1}}{2\Delta z}\right)
\end{aligned} \quad (13)$$

The algorithm for calculating the adjusted wind speed values is determined as follows:

- Obtain three-dimensional topographic data of the complex terrain.
- Develop three-dimensional discrete reliefs for finite difference method.
- Determine 3-D numerical box for finite difference method application.
- Localize measured values of wind velocities on the discrete bottom boundary of the box.
- Determine the observed wind velocities (u^0, v^0 and w^0) by least-squares method.
- Calculate the Lagrange parameters in the volume box by finite difference method.
- Use SOR method to resolve set of equations compute adjusted velocity components (u, v and w) within the box by Euler–Lagrange method (solution of the problem by variational form).

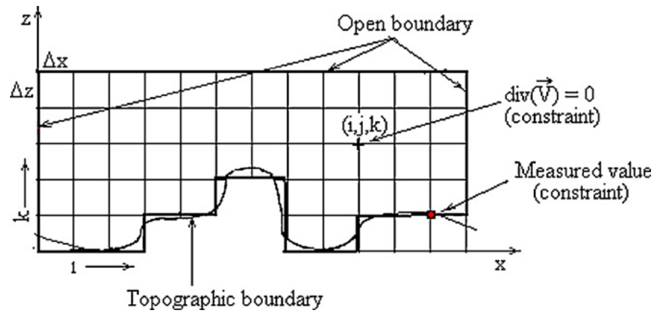


Fig. 2. Finite difference grid of the constraint problem.

3. Results and discussion

3.1. Numerical development of the terrain and grid generation

By letting x, y represent the horizontal direction and z the vertical direction over a modeling domain V, the data are arranged in the y direction and subdivided in columns. The choice of the grid size is often determined by the necessity to show the real topographic features. Fig. 2 shows a cross section of the computational volume. The topography may protrude through the top of the grid potentially producing unconnected regions within the grid volume. This feature can be used to study wind fields in valleys, canyons and mountain areas. The numerical relief shown in Fig. 3 indicates that the area of interest for this model is a rectangular box set on the earth's surface with the bottom of the box located at the lowest topographic point. The dimensions of the box are determined by the application requirements and computer storage limitations.

The computational domain is meshed by $18\times6\times10$ nodes with step $\Delta x=\Delta y=2000$ m and $\Delta z=100$ m, as shown in Fig. 3. The values of σ_1 and σ_2 were taken to be 1 and 0.01 ms^{-1}, respectively. The wind speed and direction at the upper boundary of the grid were temporally interpolated from the two vertical profile observations and assumed to be spatially constant. The horizontal wind measurements were adjusted to a height of 50 m above the terrain using a power law exponent of 0.2 [39]. The constant height interpolated and extrapolated wind field is processed to define horizontal wind components at each grid point about the topography boundary. The foregoing applications differ in terrain, meteorological data availability, meteorological condition, grid resolution, and convergence criterion.

3.2. Observed win speed and Lagrange parameters

The measured values are extracted from results of three-dimensional observed velocities ($u^0_{i,j,k}$, $v^0_{i,j,k}$, $w^0_{i,j,k}$) calculated by the AILOS software [40]. Fig. 4 shows 11 measured points (black symbols) which were chosen on the site at 10 m from the surface.

The discretised Eq. (9) is solved to give the Lagrange parameters values $\lambda_{i,j,k}$ at each node of the 3D-grid. The matrix coefficients of the equation system are diagonally dominant and asymmetric. The iterative successive over relaxation, SOR, method [37] was used to solve the correspondent equation system. Eq. (9) can be written as:

$$\lambda^{it}_{i,j,k}=(1-\omega)\lambda^{it-1}_{i,j,k}+\omega\frac{\left\lfloor A_{i,j,k}+\lambda^{it-1}_{i+1,j,k}+\lambda^{it-1}_{i-1,j,k}+\lambda^{it-1}_{i,j-1,k}++lambda^{it-1}_{i,j+1,k}+B(\lambda^{it-1}_{i,j,k+1}+\lambda^{it-1}_{i,j,k-1})\right\rfloor}{C} \quad (14)$$

where

$$A_{i,j,k}=2(\alpha_1\Delta x)^2\varepsilon_0 \quad (15)$$

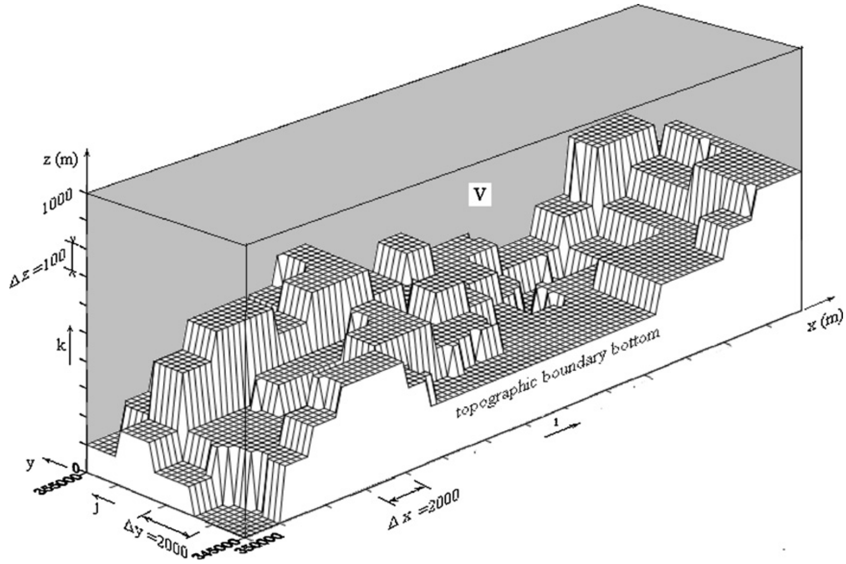


Fig. 3. Three-dimensional grid computational volume.

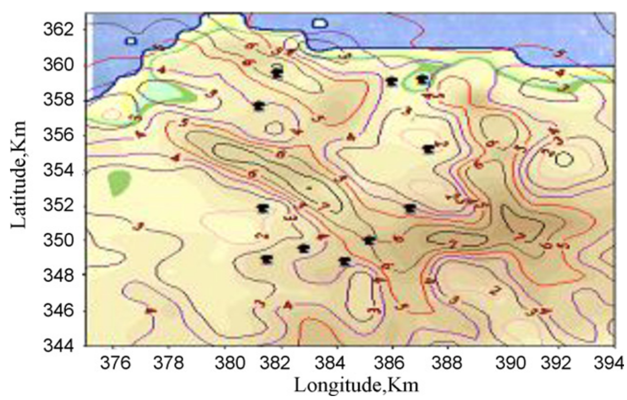


Fig. 4. Observed velocities (colored lines) calculated by AILOS software [40] and the measured points (11 black symbols). (For interpretation of the references to color in this figure legend, the reader is referred to the web version of the article.)

$$B = \alpha\left(\frac{\Delta x}{\Delta z}\right)^2 \quad (16)$$

$$C = 4\left[1 + \alpha\left(\frac{\Delta x}{\Delta z}\right)^2\right] \quad (17)$$

where $\Delta y = \Delta x$, the coefficients $A_{i,j,k}$, B and C have known values. The variable specifies the current value of the iteration in the SOR method.

The relaxation factor ω was determined experimentally and was equal to 1.78. This value is chosen so as to obtain the minimum number of iterations. The iterative solution is considered converged when the relative change of every $\lambda_{i,j,k}$ is less than a prescribed value. The iterative process is stopped when the condition on the solution accuracy is achieved

$$\left|\frac{\lambda^{it} - \lambda^{it-1}}{\lambda^{it}}\right| \prec \varepsilon* \quad (18)$$

where ε^* is a given accuracy value.

3.3. Wind speed adjusted values

The numerical technique was applied on the model as shown in Fig. 3. The study terrain was very rough, an elevation difference of over 500 m between the highest and the lowest layer was observed. The model complex relief is composed of a set of mountains or hills with a high slope. The major characteristics of the flow over a hill were determined not only by the hill shape but also by its size and by atmospheric stability. The horizontal wind measurements shown by the colored contour lines in Fig. 4 were taken from the observed velocities calculated by AILOS software in the study region of Tenes. The accuracy of the wind field is dependent on the specification of α_1 and α_2. For a stable atmosphere the horizontal adjustment were given by $\alpha_1 = 1$ and $\alpha_2 = 10$; then the adjustment is predominant in the horizontal component instead of vertical component since:

$$\alpha = \left(\frac{\alpha_1}{\alpha_2}\right)^2 = k \cdot \left(\frac{w}{u}\right)^2 = 10^{-2} \quad (19)$$

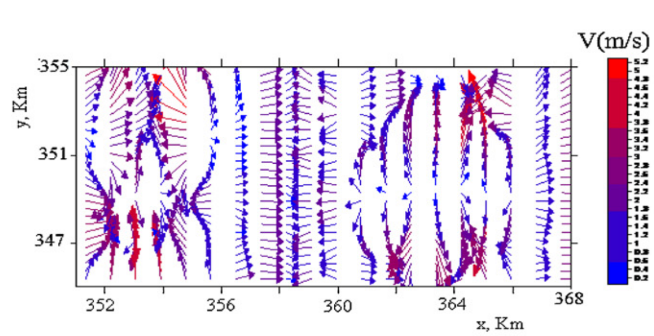
The developed computer code, applied on the numerical relief in shown in Fig. 3, produces nondivergent three-dimensional wind at 1080 grid points with the use of a Pentium 4, CPU 2.66 GHz.

3.3.1. Wind field velocity in horizontal planes

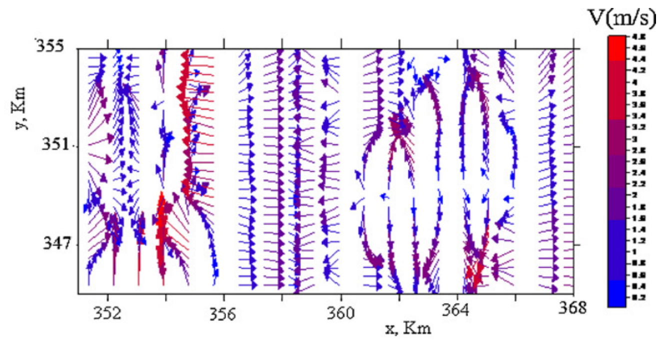
Fig. 5a shows the horizontal wind field velocity at plane (x, y) above the topographic relief. The wind values were adjusted with a step height of 100 m in the z direction using Eq. (12). The exponent p has a value of 0.2 in a period where the atmosphere was neutrally steady. The highest wind velocities were observed in the intervals [364,366] [352,356] in the x direction. An interesting area is a valley with a higher depth from the reference sea level. Fig. 5b gives the correspondent wind field which is represented by isolines of constant velocity. This gives a more precise view of the wind field velocity in the horizontal plane (x, y) than the representation of velocity given by Fig. 5a. A maximum value of the velocity reached 6 m/s in the valley at x = 366 km. It was observed that wind direction reversal occurs when the wind shifts across the valley. This outcome is also predicted by Finardi et al. [13] for a relief with a single valley. The results obtained in our study for different horizontal planes show that the rates decrease gradually as the altitude increases and become regular at an altitude of 1000 m. This is consistent with the results obtained by Sherman [19].

3.3.2. Wind field velocity in vertical planes

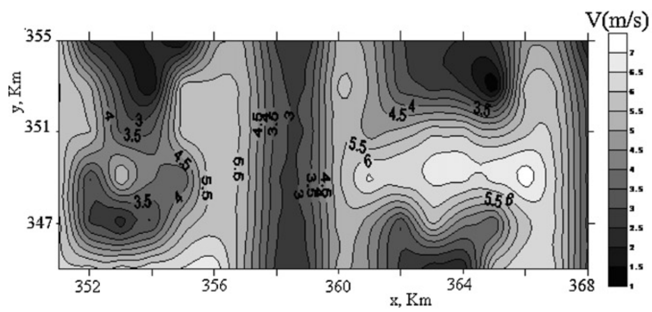
Fig. 6a–e show the velocity distribution in a vertical plane section of the computational volume and in particular the vertical motion resulting from terrain features and the wind shear present



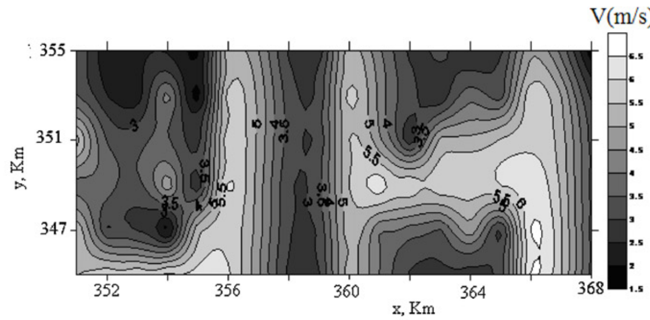
(a1) Distribution wind velocity -100 m above the topography (600 m above the reference level)



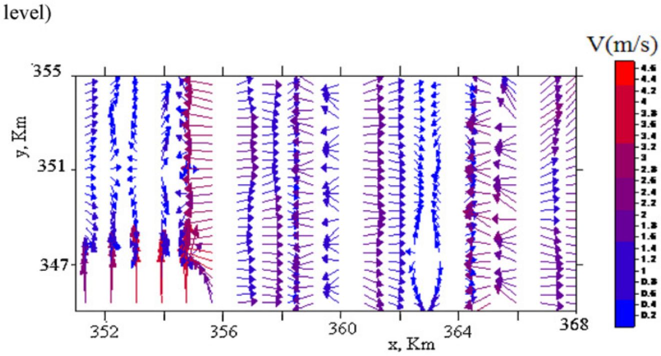
(b1) Distribution wind velocity- 200 m above the topography



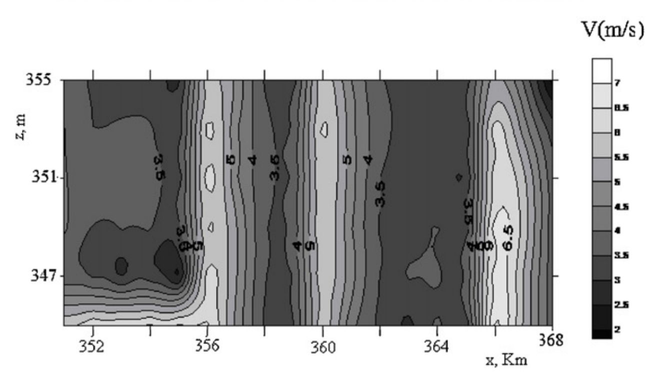
(a2) Iso-lines velocities- 100 m above the topography (600 m above the reference level)



(b2) Iso-line velocities- 200 m above the topography



(e1) Distribution wind velocity -, 1000 m above the topography

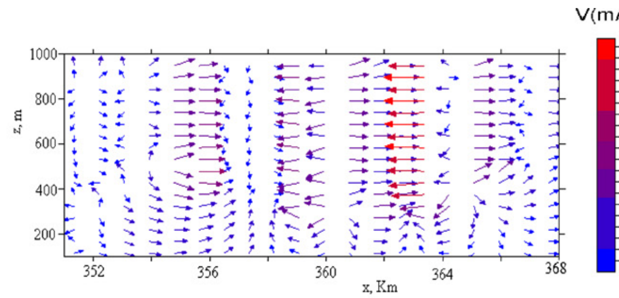


(e2) Iso-line velocities- 1000 m above the topography

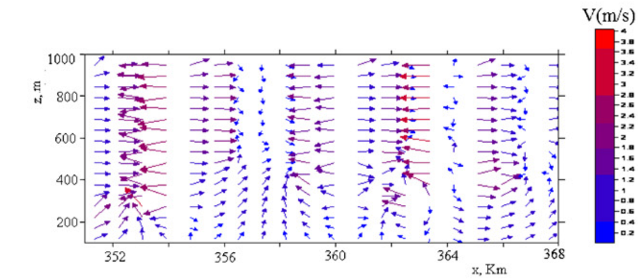
Fig. 5. Adjusted horizontal wind field in the (*x*, *y*) plan above the topography.

in the vertical profile. The field velocity decreased when the altitude increase as predicted by Equation (12); the highest velocities are located at the wall (flank) of the mountain and the area of the valley located in the intervals [364,366] [352,356] as described in section of horizontal velocities. This area indicates the location of highest power wind. These results are similar to those predicted by the two main diagnostic models; MATHEW, developed by Sherman [19] and MINERVE, developed by Geai [24] which appear to have been the more accurate and the most extensively used.

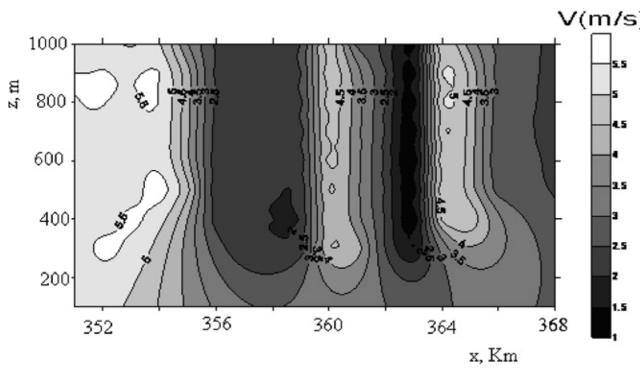
Table 2 shows the comparison of wind speeds (m/s) estimated using the current model and that estimated using Wasp for the measuring station area Tenes [41]. The current model gave a value



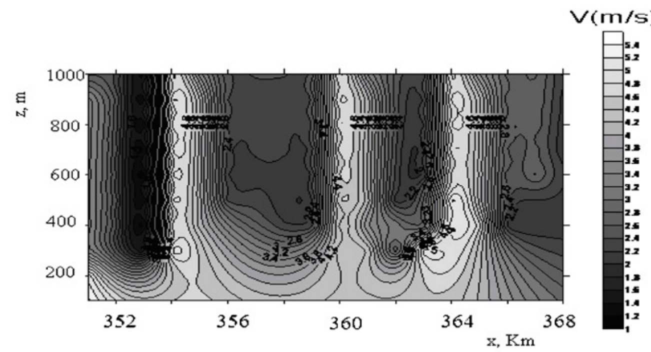
(a1) Velocity at plane y=0 (u, w wind field)



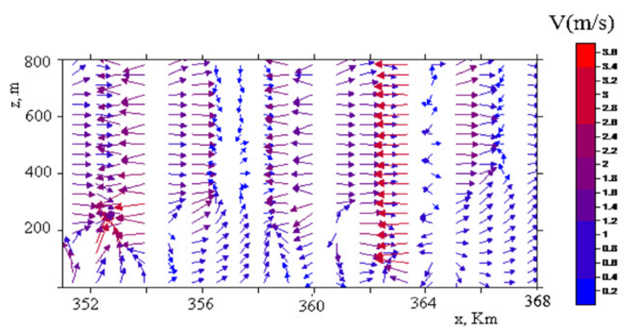
(b1) Velocity at plane y=2 Km (u, w wind field)



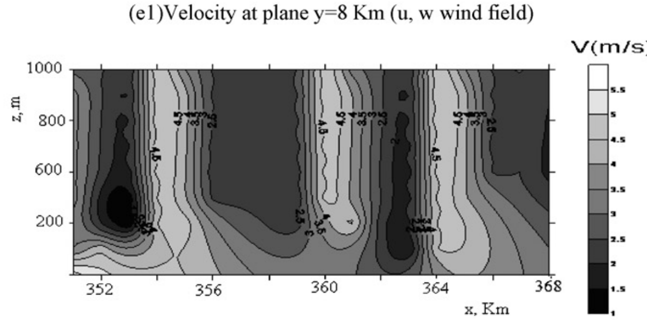
(a2) Iso-line velocity at plan y=0



(b2) Iso-line velocity at plan y=2 Km



(e1)Velocity at plane y=8 Km (u, w wind field)



(e2) Iso-line velocity at plan y=8 km

Fig. 6. Adjusted wind field velocities in the vertical (x, z) plane.

Table 2
Comparison of wind speeds estimated using the current model with that estimated by Wasp [41].

Coordinate of measurement point (m)	Present study (m/s)	Wasp (m/s) [41]	Error
(X = 3774356, Y = 356412.065,0)	3.47	3.69	−6%

of 3.47 m/s whereas the Wasp method gave a slightly higher value of 3.69 m/s [41]. It is noted that the result of the estimate based on the current model is lower by 6% compared with that predicted by Wasp.

4. Concluding remark

A numerical algorithm for the calculation of flow fields was developed. The study showed that basic optimization of constraint wind flows using a mass-consistent model is an effective method for obtaining a 3-D wind simulation over complex terrain. An application was successfully adopted for a complex terrain in the region of Tenes in Algeria. The current model gave wind speed values that were 6% lower than those estimated by Wasp software. The method allowed us to determine the windiest areas in the case study region. The precision in modeling complex terrain and the application of the scheme difference method on the topographic boundary

suggest a significant influence on the wind speed. The model developed can also be applied to dispersion of pollutants, and prediction of fire spreading.

References

[1] Boudghene Stambouli A. Promotion of renewable energy in Algeria: strategies and perspective. Renewable and Sustainable Energy Reviews 2011;15:1169–81.
[2] Himri Y, Boudghene Stambouli A, Himri S, Draoui B. Review of wind energy use in Algeria. Renewable and Sustainable Energy Reviews 2009;13:910–4.
[3] Himri Y, Himri S, Boudghene Stambouli A. Assessing the wind energy potential projects in Algeria. Renewable and Sustainable Energy Reviews 2009;13:2187–91.
[4] Himri Y, Himri S, Boudghene Stambouli A. Prospect of wind farm development in Algeria. Desalination 2009;239(1–3):130–8.
[5] Wang X, Peper DW. A mass consistent atmospheric using FEMLAB optimization. In: Excerpt from the proceedings of the COMSOL multiphysics user's conference. 2005.
[6] Mortensen NG, Petersen EL. Influence of topographical input data on the accuracy of wind flow modeling in complex terrain. In: Proceedings of the 1997 European wind energy conference and exhibition. 1997. p. 317–20.
[7] Shafie-Pour M, Rashidi Y, Ardestani M. Simulation of wind field in Teheran using Hybrid Diagnostic Prognostic Model. American Journals of Environmental Sciences 2008;4(5):512–21.
[8] Ludwig FL, Byrd G. An efficient method for deriving Mass-Consistent flow fields from wind observations in rough terrain. Atmospheric Environment 1980;14:585–7.
[9] Ivancie M, Rakovec J. Diagnostic wind field, seminar. University of Ljubljana, Faculty of Mathematics and Physics; 2010.
[10] Lee M, Lee1 SH, Hur1 N, Choi C-k. A numerical simulation of flow field in a wind farm on complex terrain. In: The seventh Asia-Pacific conference on wind engineering, November 8–12. 2009.
[11] Wang Y, Williamson C, Huynh G, Emmitt D, Greco S. Diagnostic wind model initialization over complex Terrain using the air borne Doppler wind lidar data. The Open Remote Sensing Journal 2010;3.
[12] Flores C, Juárez H, Núñez MA, Sandova ML. Algorithms for vector field generation in mass consistent models, Numerical method for partial differential equation. Article first published online: 9 APR; 2009. doi:10.1002/num.20458. Copyright © 2009 Wiley Periodicals Inc.
[13] Finardi S, Grazia Morselli M, Jeannet P. Wind flow models over complex terrain for dispersion calculations, cost action 710, pre-processing of meteorological data for dispersion models. Report of Working Group 4; May 1997, COST 710 WG 4.
[14] Mocioaco G, Svertsen B, Cuculeanu V. Three dimensional wind field estimates in complex terrain. Romanian Reports 2009;61(2):281–92.
[15] Christiane M. Simulation over atmospheric flows over complex terrain for wind power potential assessment. Thèse de Doctorat Es Science, No 1855, Ecole Polytechnique Lausane, Swiss; 1998.
[16] Sasaki Y. An Objective Analysis based on the variational method. Journal of the Meteorological Society of Japan 1958;36:77–88.
[17] Sasaki Y. Some basic formalism in numerical variational. Monthly Weather Review – Japan 1970;98:875–83.
[18] Sasaki Y. Numerical variational analysis formulated under constraint determined by Long wave equation and low pass filter. Monthly Weather Review – Japan 1970;98:884–98.
[19] Sherman CA. A mass consistent for wind fields over complex terrain. Journal of Applied of Meteorology 1978;17:312–9 (Mathew).
[20] Dickerson MH. MASCON – a mass consistent atmospheric flow model for regions with complex terrain. Journal of Applied of Meteorology 1978;17:241–53 (Mascon).
[21] Phillips GT. A preliminary user's guide for the (NOABL) objective analysis code. Technical report DOE Contract AC06-77/ET/20280, NTIS U.S. Dept. of Energy, Springfield, Virginia; 1979 July.
[22] Endlich RM, Ludwig FL, Bhumralkar CM. A diagnostic model for estimating. Winds at potential sites for wind turbines. Journal of Applied of Meteorology 1982;21:1441–54 (Complex).
[23] Davis CG, Bunker S, Mutshleener S. Atmospheric transport models for complex. Journal of Climate and Applied Meteorology 1984;23:235–8 (ATMOS1).
[24] Geai P. Méthode d'interpolation et de reconstitution tridimensionelle d'un champ de vent: le code d'analyse objective MINERVE, Report EDF/DER, HE/34-87.03; 1987.
[25] Moussiopoulos N, Flassak T, Sahm P, Berlowitz D. A refined a diagnostic wind field model. Environmental Software 1988;3:85–94 (Condor).
[26] Ross DG, Smith IN, Manins PC, Fox DG. Diagnostic wind field modelling for complex terrain: Model development and testing. Journal of Applied of Meteorology 1988;27:785–96 (NUATMOS).
[27] Ratto CF, Festa R, Nicora O, Moseillo R, Ricci A, Lala DP, et al. Wind field numerical simulations anew user friendly code. In: Palz W, editor. European community wind energy conference. 1990.
[28] Ludwig FL, Livingston JM, Endlich RM. Use of mass conservation and critical dividing streamline concepts for efficient objective analysis of winds of complex terrain. Journal of Applied of Meteorology 1991;30:1490–9 (WOCSS).
[29] Wang X, Peper DW. A mass consistent atmospheric using FEMLAB optimization. In: Excerpt from the proceedings of the (COMSOL) Multiphysics User's conference, vol. 14. 2005.
[30] Ratto CF, Festa R, Romeo C, Frumento OA, Galluzzi M. Mass consistent Models for wind fields over complex terrain: the state of the art. Environmental Software 1994;9:247–68.
[31] Chan ST, Sugiyama G. A new model generating mass consistent wind fields over continues terrain. In: American nuclear society's sixth topical meeting on emergency preparedness and response. 1997.
[32] Leone JM, Nasstrom JS, Maddix D. A first look at the New ARAC dispersion model. In: Sixth topical meeting on emergency preparedness and response. 1997.
[33] Ross DG, Fox DG. Evaluation of an air pollution analysis system for complex terrain. Journal of Applied of Meteorology 1991;30:909–23.
[34] Ishikawa H. Mass-consistent wind model as a meteorological pre-processor for tracer transport models. Journal of Applied of Meteorology 1994;33: 733–43.
[35] Boukli Hacène F, Kasbadji Merzouk N, Loukarfi L. Analyse statistique et Elaboration d'un atlas éolien de la vallée du Chéliff. Revue des Energies Renouvelables 2007;10(4):583–8.
[36] National Meteorology Office, NMO. Base de données des vitesses du vent. station de Chlef; 2001–2005.
[37] M. Tahar Abbes, Méthodes Numériques, Office des Publications Universitaires (OPU); 2007. ISBN 978-9961-0-1065-5.
[38] Justus CG, Mikhaïl SS. Height variation of wind speed and wind speed distribution Statistics. Geophysical Researchers Letters 1976;3(5).
[39] Kasbadji Merzouk N, Merzouk M, Messen N, Benyoucef B. Profil vertical de la vitesse du vent en milieu semi aride-test des modèles d'extrapolation. In: Proceeding International Congress on photovoltaic and Wind Energies, Tlemcen, Algeria; 2003.
[40] Kasbadji Merzouk N. Evaluation du gisement éolien, contribution à la détermination du profil vertical de la vitesse du vent en Algérie. Doctorate thesis, Tlemcen, Algeria; May 2006.
[41] Abdeslam D, Kherba N, Boukli Hacène F, Kasbadji Merzouk N, Merzouk M, Mahmoudi H, Goosen M. On the use of the wind energy to power reverse osmosis desalination plant: a case study from Ténès (Algeria). Renewable and Sustainable Energy Reviews 2011;15:956–63.
[42] Homicz GF. Three-dimensional wind field modeling: a review. SAND REPORT SAND2002-2597 unlimited release printed; August 2002.